IMPROVING URBAN VEGETATION CLASSIFICATION ACCURACY WITH MULTISPECTRAL IMAGERY AND LIDAR

THESIS

Presented to the Graduate Council of
Texas State University-San Marcos
in Partial Fulfillment
of the Requirements

for the Degree

Master of SCIENCE

by

Guinevere McDaid, B.S.

San Marcos, Texas
August 2013

IMPROVING URBAN VEGETATION CLASSIFICATION ACCURACY WITH MULTISPECTRAL IMAGERY AND LIDAR

Committee Members Approved:

Jennifer L. Jensen, Chair

Edwin T. Chow

Yongmei Lu

Approved:

J. Michael Willoughby
Dean of the Graduate College

FAIR USE AND AUTHOR'S PERMISSION STATEMENT

Fair Use

Duplication Permission

ACKNOWLEDGEMENTS

The researcher would like to thank her Academic Adviser, Dr. Jennifer Jensen, for all of her support and guidance throughout this process. The researcher is especially appreciative of the consistently constructive and punctual feedback provided by her adviser on the multiple research drafts that were submitted for edits and always returned within a matter of days. This allowed her to maintain a consistent level of motivation and momentum which in turn facilitated the timely completion of this work.

The researcher would also like to acknowledge the beneficial influences of her two committee members, Dr. Edwin Chow and Dr. Yongmei Lu for their vital contribution of unique expertise to the production of this research.

Lastly, the researcher would also like to thank her roommate Cole Parker, her father Brendan McDaid and her sister, Daphne McDaid for all of the support and understanding they provided throughout her graduate school journey.

This manuscript was submitted on June 14, 2013.

TABLE OF CONTENTS

Page

LIST OF TABLES

Table **Page**

LIST OF FIGURES

Figure **Page**

LIST OF EQUATIONS

ABSTRACT

IMPROVING URBAN VEGETATION CLASSIFICATION ACCURACY WITH MULTISPECTRAL IMAGERY AND LIDAR

By

Guinevere McDaid

Texas State University-San Marcos

August 2013

SUPERVISING PROFESSOR: JENNIFER JENSEN

Urban areas are comprised of fine-scale heterogeneous land-cover classes and detailed land cover classifications often require multiple techniques and classification methods to produce an accurate land cover land-use map. Policy makers and urban developers need up-to-date, precise data in which to base decisions and to guide development decisions that meet multiple objectives. Accurate and up-to-date land cover data, particularly in rapidly developing cities, is often unattainable at the spatial resolution desired by urban planners. Aerial remote sensing is a suitable and effective source for urban land cover mapping as the image datasets for classification are acquired at a high spatial resolution (e.g., 1 m). This study examines added utility of integrating1 m image data, lidar height data, and lidar intensity data as a means of increasing the classification accuracy of urban vegetation classes compared with that of a classification using aerial image data alone. One meter National Agricultural Inventory Program (NAIP) data, acquired in 2010 were used as input to an object-oriented, supervised classification in ENVI EX to derive urban vegetation land cover in the downtown area of San Antonio, Texas. Classification of data adhered to the Texas Land Classification System (TXLCS). The classes used here include developed, developed open-space,

broad-leafed evergreen, cold deciduous, mixed forest, and shadows. These analyses indicate that the addition of lidar height data as a classification layer did not improve classification accuracy compared to image data alone. The addition of lidar intensity data as a classification layer did however improve the classification accuracy compared to image data alone. The integration of spectral and intensity data does produce a more accurate urban vegetation land cover map.

1.0 INTRODUCTION

1.1 Background

Urban areas constitute spectrally heterogeneous land-cover classes and call for the application of multiple techniques and classification methods to produce an accurate land cover land-use (LCLU) map. Policy makers and urban developers need up-to-date, precise data in which to base decisions and regulations on as well as guidelines as to where new development should occur in relation to existing features on the surrounding landscape. High resolution, up-to-date land cover data, particularly in rapidly developing cities, is often unavailable. To solve this deficiency in information availability, aerial remote sensing is a suitable and effective source for urban land cover mapping.

Urban areas are one of the fastest growing and constantly changing land cover types in the world. Recent efforts to build, develop, and create environmentally sustainable cities equipped to adequately provide suitable living environments for the rapidly growing urban populations are exacerbating the rate of change in which we are witnessing across these urban landscapes. For example, there has been a recent move towards mitigating urban heat island effects by using newly developed roofing materials designed to reflect more sunlight than the more traditionally used dark building material (Kleerekoper et al., 2012). There has also been an increase in the amount of urban trees added to urban areas to provide for more temperature regulating effects (Solecki et al., 2005). Although these changes to urban landscapes are generally considered to be

beneficial, it has changed the way that urban features on the landscape are classified. For example, a green roof or living roof is partially or completely covered with vegetation and could potentially be misclassified as some type of vegetated area as opposed to a building. Efforts to develop new methods or alter existing techniques are warranted to create accurate and high-resolution land cover maps, especially for these urban areas.

1.2 Problem Statement

The current literature has demonstrated that land cover classification accuracy is considerably improved when light detection and ranging (lidar) derived information is added to spectral information for the purpose of classifying land cover (Bork and Su, 2007; Grebby et al., 2011; Mesas-Carrascosa et al., 2012). The greatest increase in accuracy occurs when classifying highly variable or spectrally heterogeneous land cover types like those found in dense urban areas. Many studies have explored methods to improve the classification accuracy of urban features, such as roads and buildings. There have also been considerable efforts to increase the classification accuracy between plant species in non-urban environments; however, few studies have focused on improving the accuracy between urban vegetation classes.

1.3 Objective

The research objective is to determine if land cover classification accuracy of a high resolution aerial image is significantly improved when lidar derived information is included in the classification process. This will be determined by creating two urban land classification maps. Specific classes developed by the (USGS) Land Classification System will be used. The image only and image plus lidar classification accuracy

assessments will be compared to determine if the addition of lidar data improves product accuracy.

1.4 Justification

Recent studies have demonstrated the advantages of combining imagery and lidar data to perform urban land cover classifications, especially for providing increased class separability between spectrally similar classes like buildings and roads (Chen et al., 2009; Mallet et al., 2008; Huang et al., 2011). Efforts have been made to improve the classification of individual tree species using this combinative approach (Bork and Su, 2007; Popescu and Zhao, 2008; Ke et al., 2010; Dalponte et al., 2012; Cho et al., 2012; Heinzel and Coch, 2012). However, studies to improve the accuracy of urban vegetation classifications outside of the discrimination between vegetation and non-vegetation classes are lacking, and thus the justification for this research.

Numerous forest related studies (Song et al., 2002; Brandtberg et al., 2003; Holmgren and Persson, 2004; Donoghue et al., 2007; Kim et al., 2009; Heinzie and Koch, 2012; Yao et al., 2012) have demonstrated the usefulness of lidar data to provide further discrimination between spectrally similar vegetation species, especially when combined with image data (Dalponte et al., 2012). Therefore, it is reasonable to assume that the use of this integrative approach will increase the class separability between urban vegetation.

2.0 LITERATURE REVIEW

2.1 Multispectral Image Classification

Advances in the classification of multispectral imagery for the creation of land cover land-use (LCLU) maps emerged in the early 1990s and gained recognition as a powerful research tool across a range of disciplines. Some studies focused on research relating to forest cover mapping (Niemann, 1993; Danson et al., 1993; Adams et al., 1995; Martin et al., 1998), vegetation mapping (Pickup et al. and Henebry, 1993; Pons and Solé-Sugrañes, 1994; Muller, 1997; Kadmon and Harari-Kremer, 1999), geomorphology (Singh et al., 1993; Mantovani et al., 1996; Walsh et al., 1998; Froger et al., 1998) and urban development (Eyton, 1993, Aniello et al., 1995; Barnsly and Barr, 1997; Ridd, 1998). By the start of the twenty-first century, a rapid increase in the number of satellites capable of acquiring multispectral image data allowed for even further expansion of land cover land-use research. For example, during the year 2000, sensors such as ASTER (Advanced Spaceborne Thermal Emission and Reflection Radiometer) and MODIS (Moderate Resolution Imaging Spectroradiometer) which are both mounted on the Terra satellite platform, as well as Hyperion and ALI (Advanced Land Imager) mounted on the EO-1 (Earth Observation 1) platform all became available sources for multispectral image acquisition. In 2001, MODIS mounted on the Aqua platform was also launched.

Over the last 12 years, extensive research into topics such as floodplain mapping (Straatsman and Baptist, 2008; Chormanski et al., 2011), urban sprawl (Jacquin et al., 2008; Schneider 2012) , urban heat island effects (Weng et al., 2004; Onishi et al., 2010), habitat modeling (Stow et al., 2008; Hamada et al., 2011), and climate change (Raup et al., 2005; Katra and Lancaster, 2008) have emerged as common research themes with regard to multispectral image classification. For example, Forzieri et al. (2012) performed multiple types of land classifications on SPOT-5 multispectral image data in order to identify and quantify the vegetation hydrodynamic parameters across the landscape. The authors successfully showed that their new method of floodplain roughness parameterization could provide accurate hydraulic output and enhance the roughness estimation. Shahraki et al. (2011) used Landsat image data acquired on four different dates to quantify urban sprawl that has occurred over the last 35 years in the Iranian city of Yazd. Landsat TM images were used by Guo et al. (2012) to classify and quantify the magnitude of urbanization in Beijing, China based on land cover-specific surface temperatures. Culbert et al. (2012) successfully model avian species biodiversity across the Midwestern United States based on multispectral image texture parameters. All-in-all, a diverse set of basic and applied research has emerged due to the availability of multispectral image datasets.

2.2 Lidar-based Classification

On the other hand, lidar data provide georeferenced, irregularly distributed 3D point clouds of high altimetric accuracy (Guo et al., 2011). Similar to radar, lidar is able to record 3D information about topographic features, structures, and landscapes. Lidar systems can provide either single laser pulse returns or multiple returns that correspond to

the respective object's height and structural characteristics. In addition to the multiple return lidar systems, full-waveform (FW) systems are able to record one dimensional signals that represent a continuous arrangement of echoes caused by reflections from different targets (Chehata, 2009). Waveform systems offer more information about the target feature and the physical characteristics of the area surrounding it since the entire return signal is digitized.

Research involving the use of lidar data for classification includes the mapping of coral reefs and shallow water habitat modeling (Wedding et al., 2008; Chust et al. 2010; Collin et al., 2010; Tulldahl and Wikström, 2012) of coastal environments. Continuous improvements to lidar systems have allowed for precise as well as increasingly affordable data to become available, especially over large areas.

The use of lidar systems began with the National Aeronautics and Space Administration (NASA) program in the 1970s, but it was not until the implementation of the Global Positioning System (GPS) in the late 1980s that the accurate positioning needed for high-performance lidar systems became available (Renslow, 2000). Even then, highly accurate real-time GPS recording was not publically available until selective availability was turned off in 2000 by the Clinton administration. Prior to 2000, land classification studies using lidar data are sparse in the literature because the technology was not commonly available for use. However, at present, there is no shortage of current research evaluating the wide range of potential usages that lidar can facilitate.

2.3 Lidar for Vegetation Discrimination

Since vegetation exhibits similar spectral properties (e.g., high reflectance in the near infrared wavelengths and low reflectance in the blue and red wavelengths) the instance of class overlap and subsequent misclassification can be problematic. Accurate land classification using multispectral data is variably limited to distinguishing classes based on only a small range of variance between the spectral properties. This is partly why lidar research has progressed so rapidly in forest management-related research. Due to its unique ability to measure objects on the Earth's surface in three dimensions, lidar has the capability to acquire structural information about vegetation like tree height, crown area, and crown base height which can be used to further distinguish between spectrally similar vegetation types. Individual trees have a diverse crown architecture that depends on species, age, position within the canopy, leaf-on/leaf-off conditions, and position of small gaps within tree crowns (Popescu et al., 2008). Research by Brandtberg et al. (2003) used indices derived from laser reflectance data as well as height of branches to classify three different deciduous species. Holmgren and Persson (2004) used two groups of variables, crown shape-based metrics and intensity-based metrics, to differentiate Norway spruce and Scots pine.

Donoghue et al. (2007) evaluated the ability of lidar data to estimate the proportion of species in pine/spruce mixed plantations. They used lidar intensity to separate spruce and pine species and found that the coefficient of variation and lidar intensity were the most useful predictors of the proportion of spruce. Song et al. (2002) applied filters to a gridded representation of intensity data and concluded that the relative intensity of (leaf-on) broadleaved trees was almost twice that of conifers. Kim et al.

(2009) investigated the combined use of leaf-on and leaf-off lidar datasets for their tree species study. They evaluated lidar intensity values of multiple coniferous and deciduous tree species with different foliage characteristics, such as the presence or absence of foliage, and the spacing and type of foliage components within individual tree crowns. They also examined the relative importance of the effects of these characteristics on lidar-based species classification. Heinzie and Koch (2012) tested multiple complex tree feature combinations derived from FW lidar data in order to determine which lidar derived variables were the best to maximize the classification accuracy for six different tree species. Yao et al. (2012) also used FW lidar derived tree shape parameters to perform a species classification on deciduous and coniferous trees.

Ke et al. (2009) evaluated the effects of adding lidar data to multispectral data for the improvement of forest species classification. They showed that combining multispectral and lidar data together, in both image segmentation and object-based classification, improved their forest classification accuracy by 20 percent compared to using only multispectral data.

2.4 Urban Classification with Multispectral and Lidar Data

Research focused on urban feature extraction via multi-source remotely sensed data fusion emerged in the literature in the early 1990s. For example, Haala (1994) performed feature extraction of buildings by fusing lidar and multispectral data together. Later, Haala (1997) conducted a pixel-based unsupervised urban land use classification using Geographic Information Systems (GIS), high spatial resolution stereo and multi-spectral images recorded from a Digital Photogrammetric Assembly (DPA) scanning airborne sensor. In 2002, McIntosh and Krupnik used the addition of aerial imagery to

create a refined digital surface model (DSM) originally created from lidar data alone in an attempt to increase the accuracy. By merging the edge information from the imagery with the lidar data, the authors were able to create a better representation of surface discontinuities and improved surface accuracies.

In an effort to address these issues that are indicative of complex urban feature classification, a surge in lidar related analyses and techniques emerged during the beginning of the twenty first century. The most widely used application of lidar data is to generate digital elevation models (DEMs) (Liu, 2008) which are 3D representations of a terrain surface. Two of the most commonly used DEMs are digital surface models (DSMs) which represent the terrain including all objects on it (e.g., buildings and vegetation) and digital terrain models (DTMs) which represent the terrain without surface features.

Axelsson (2000) and Vosselman and Mass (2001) both evaluated classification approaches that use a Triangulated Irregular Network (TIN) data structure to create DEMs for urban areas. Axelsson's work focused on the creation of DEMs of very high density and accuracy by applying an adaptive TIN model designed for use on very discontinuous surfaces such as dense cities. Vosselman and Mass (2001) evaluated the use of a slope-based filtering algorithm that uses mathematical morphology capable of filtering out vegetation points while keeping building points. Ameri (2000) and Al-Harthy and Bethel (2002) explored building extraction techniques using the difference between DSMs and DTMs.

Zhou (2004) combined lidar data and orthoimagery for urban 3D digital building model (DBM), DSM and DTM generation. Initially, an image processing for edge detection was conducted from orthoimagery; image interpretation was performed to extract the buildings, trees, roads, etc., and then to integrate the image knowledge into lidar point cloud for the generation of a 3D DSM, DTM, and DBM.

In Gross et al. (2007) and Wagner et al. (2008), geometric and FW lidar features were derived from a FW 3D point cloud and used to distinguish between vegetation and non-vegetation points within urban areas. Rutzinger et al. (2008) presented an object-based analysis of a FW lidar point cloud to extract urban vegetation. First, the 3D point cloud was slightly over-segmented using a seeded region growing algorithm based on the echo width. Each segment was then statistically analyzed in order to compute selected point features which included amplitude, echo width, and geometrical attributes. A supervised classification per statistical tree decision was then applied.

Huang et al. (2011) used lidar data as a complementary source to spectral signals to improve the accuracy of land cover mapping in urban areas. They used feature extraction algorithms combined with lidar-derived spectral information in their study. Hofle and Hollaus (2010) calculated an enhanced echo ratio feature which resulted in improved vegetation discrimination. Mallet et al. (2008) improved a rule-based classification using fix echo amplitude and width to differentiate non-vegetation features such as roof edges, building walls, and power lines.

Guo et al. (2011) examined the relevance of multi-source data composed of lidar features (multiple return and FW) and multispectral RGB bands for mapping urban

scenes using the Random Forest classifier algorithm. In this study, four classes were created; buildings, vegetation, artificial ground, and natural ground and the Random Forests classifier algorithm was used. According to the authors, this algorithm is appropriate for use with a multi-source framework and is able to process large datasets. Chen (2009) compared the accuracy between classifying urban landscapes using a traditional pixel-based approach with an approach that integrated the addition of lidar derived height data. The authors' goal was focused on increasing the accuracy of the building and road classes. In total, nine land cover classes (water, shadow, vegetation, shrub, and grassland, high building, low building, road, and vacant land) used which were extracted one by one using different segmentation parameters. For example, from Quickbird imagery, Normalized Difference Water Index (NDWI), Seasonal Shift Index (SSI), and Normalized Difference Vegetation Index (NDVI) were used to delineate shadow, water, shrub, grassland, vacant land, and road pixels and a DTM and DSM created from the lidar data were used to identify high buildings, low buildings, and roads. The comparison of the classification accuracy between these methods resulted in an overall accuracy increase from 69.12 percent (pixel-based approach) to 89.40 percent (pixel-based approach combined with lidar height data).

Several studies have used the fusion of lidar derived canopy height models (CHMs) with multispectral data to improve the separability between rooftops, roads, and buildings that are commonly misclassified due to their similar spectral and spatial characteristics (Lee and Shan, 2003), (Alanso and Malpica, 2008), and (Rottensteiner et al., 2005). The inclusion of canopy surface models (CSM) have also proved useful but require a labor intensive process of classifying lidar point data into ground and non-

ground returns (Lefsky et al., 2002; Meng et al., 2010). Hartfeild et al. (2011) used a lidar derived CHM, lidar intensity and height data along with multispectral image data for an urban land classification, but also expanded their study to include the classification of seven other classes for the purpose of modeling suitable urban mosquito habitat. In their study, Classification and Regression Tree (CART) analyses were used to compare the enhancements and accuracy of a multi-sensor urban land cover classification but more specifically to evaluate how adding elevation and attribute height data extracted from the lidar data would help to discriminate attributes such as buildings, roads, and the often dry streams and waterways. The results of their study demonstrated that the combined use of lidar data and multispectral imagery along with NDVI data improved the accuracy of their urban land classification. Lastly, Charaniya et al. (2004), combined lidar intensity data, a digital elevation model (DEM), and black and white photography to successfully distinguish between grass, trees, asphalt, and rooftops.

3.0 METHODOLOGY

3.1 Study Area

The study area focuses on the north-east section of downtown San Antonio which is located in Bexar County, Texas (Figure 1). There is a mixture of broad-leaf evergreen and deciduous trees. There is only one predominant broad-leaf evergreen species, which is the Live Oak, within the study area with the occasional Mexican White Live Oak. Within the deciduous forest class there are over ten deciduous tree species dispersed throughout the study area which are listed in Table 1.

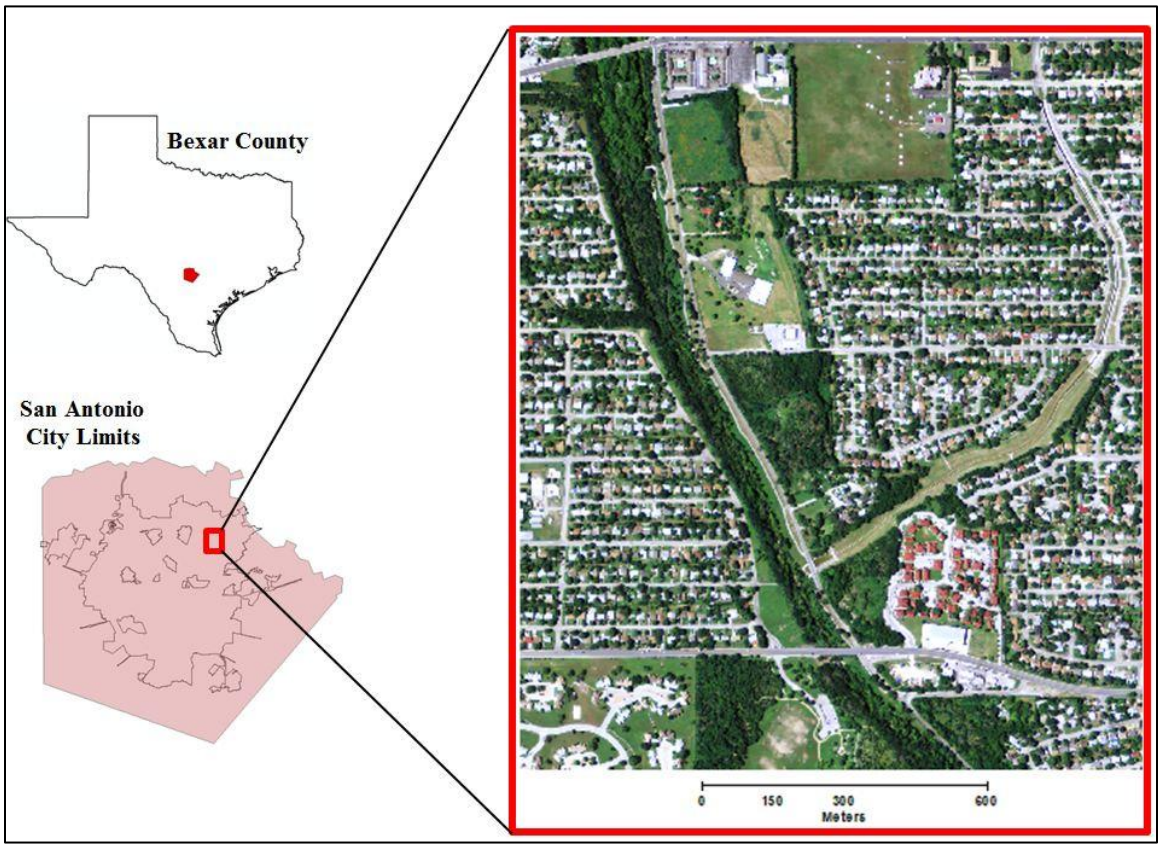

Figure 1. Study area in north east downtown San Antonio, Texas

Table 1. Land-cover class descriptions for the north east section of San Antonio

Land Cover Class	Description
Developed	Includes highly developed areas where people reside or work in high numbers. Examples include apartment complexes, row houses and commercial/industrial. Impervious surfaces account for 80 to100 percent of the total cover.
Developed Open-space	Includes areas with a mixture of some constructed materials, but mostly vegetation in the form of lawn grasses. Impervious surfaces account for less than 20 percent of total cover. These areas most commonly include large-lot single-family housing units, parks, golf courses, and vegetation planted in developed settings for recreation, erosion control, or aesthetic purposes.
Broad-leaved Evergreen Forest	Area dominated by evergreen trees that have well-defined leaf blades and are relatively wide in shape. Example species include *Quercus virginiana* var. *fusiformis*.
Cold Deciduous Forest	Area dominated by trees that shed their leaves as a strategy to avoid seasonal periods of low temperature. Example species include: *Platanus mexicana, Lagerstromia indica, Carya illinoensis, Quercus macrocarpra, Quercus muehlenbergi, Quercus laceyl, Quercus buckleyi, Juglans microcarpa, Ulmus crassfolia, Acer grandidentatum, Prosopis glandulosa*
Mixed Forest	Areas dominated by trees where neither deciduous nor evergreen species represent more than 75% of the canopy cover.
Shadow	Shadows

3.2 Site Selection

The study site selection was based on the presence of a wide variety of urban features and urban vegetation types located within this study area. The land cover classes used here are based on the National Land Cover Datasets Level II classification system and include developed, developed open-space, broad-leafed evergreen forest, cold-deciduous forest, mixed forest, and shadow. A detailed description of these land cover classes is provided in Table 1. The study area covers a total area of 206 hectares.

3.3 Lidar Data Collection and Processing

The lidar data used for this study were commissioned by the Texas Water Development Board (TWDB) in conjunction with the San Antonio River Authority (SARA) for the purpose of supporting flood mapping throughout Bexar County. It was collected in October of 2010 during leaf-on season. High density lidar data were acquired over the study area with a Terrapoint Mid-Range sensor mounted to a Pipper Navaho airplane. The lidar acquisition parameters are provided in Table 2. The lidar vendor, Terrapoint, provided raw lidar data consisting of *XYZ* coordinates, off-nadir angle, and intensity information for all lidar returns within the area. Raw elevation measurements were tested against 18 Terrapoint-acquired static GPS points based on the National Standard for Spatial Data Accuracy (NSSDA) standards. The classification of the lidar mass point cloud into ground and non-ground was also provided by the vendor along with a gridded DEM, hydro flattening breaklines, contours, and intensity information. The generation and calibration of the lidar data was done using Terrapoint's

proprietary laser post-processing software for Midrange data. This software combines the raw laser range and angle data file with the finalized GPS/IMU trajectory information.

Table 2. Lidar acquisition parameters

Acquisition Parameters	
Collection date	October 2010
Aircraft	Piper Navaho
Sensor	Terrapoint Mid-Range
Flight height above mean terrain (m)	600
Laser pulse density/ (m^2)	5
Laser pulse rate (kHz)	150
Swath width (m)	692
Scan angle from nadir (°)	±30
Horizontal accuracy (m)	0.01
Vertical Accuracy (m)	0.19

3.4 NAIP Image Data and Processing

Imagery used for this study came from the National Agriculture Imagery Program (NAIP). NAIP acquires one meter resolution digital orthoimagery during the agricultural growing seasons in the continental U.S. A primary goal of the NAIP program is to enable the availability of orthoimagery within one year of acquisition, however, for the purpose of this study, imagery that was acquired in May 2010 was used as it temporally coincided with the 2010 lidar data acquisition.

One meter aerial image data were collected using a Leica ADS80 digital sensor and then downloaded using Leica XPro software. The raw imagery was then georeferenced using GPS/INS 200Hz exterior orientation (EO) information (x/y/z/o/p/k). Tie points in three bands/looks (Back/Nadir/Forward) for each flight line were measured using Leica Xpro software. The resulting point data and EO data was then used to perform a full bundle adjustment. Any blunders were removed, and weak areas were manually enhanced to ensure good coverage of points. Once the cleaned point data and point coverage was considered acceptable, photo-identifiable GPS-surveyed ground control points were introduced in the corners and center of the block being adjusted. The output from this bundle adjustment process is the revised exterior orientation data for the sensor with any GPS/INS, datum, and sensor calibration errors modeled and compensated for. Using this revised EO data orthorectified image strips are created using the USGS NED DEM. The orthorectified strips were overlaid with each other and with the ground control to check for accuracy. Once the accuracy of the orthorectified image strips were validated , they were processed with a NWG proprietary dodging package that

compensates for the bi-directional reflectance function that is caused by the sun's position relative to the image area. This compensated imagery is then imported into Inpho's OrthoVista 4.4 package which is then used for the final radiometric balance, mosaic, and digital ortho quarter quad (DOQQ) sheet creation (Figure 2). These final DOQQ sheets contain a 300 m minimum buffer and are edge inspected to the existing mosaicked DOQQ sheets for accuracy validation. Each individual image tile within the mosaic covers a 3.75 x 3.75 minute quarter quadrangle. The DOQQs are delivered in GeoTIFF format and the area corresponds to the USGS topographic quadrangles. The positional accuracy of the NAIP imagery has an overall root mean square error (RMSE) of 1.24 meters (USDA-FSA-APFO Aerial Photography Field Office, 2010).

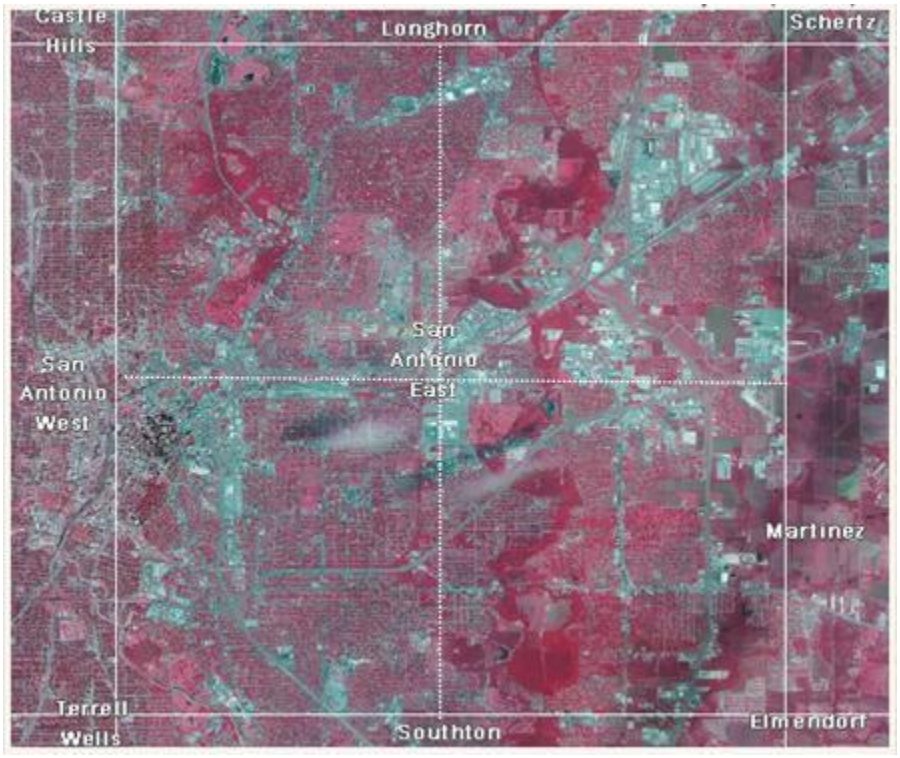

Figure 2. Orthoimagery following the standard USGS Quarter Quad Grid

3.5 Analysis Procedures

Using ENVI EX, three object-oriented classifications were performed and presented here; imagery alone, imagery plus lidar-derived height information, and imagery plus lidar-derived intensity information. ENVI EX is an object-oriented classification software that allows for feature extraction from spectral and spatial datasets. It segments an image into regions of pixels by evaluating the attributes of each region to create distinct objects, and then classifies the objects to extract features of interest. The alternative, manual location and digitization of features in an image is tedious and time consuming, especially over large areas. Additionally, traditional pixel-based extraction approaches are limited to classifying based solely on spectral characteristics of an image which can be less accurate when using multispectral images that are highly heterogeneous like urban areas. The automated workflow of ENVI EX (Figure 3) leads you through each step of the feature extraction process with dialog boxes and preset, but adjustable parameters. Following image segmentation, a choice is given to either select specific training objects in the image that represent each class or a rule-set can be created that specifies certain parameters that an object must have in order to be assigned to a class. For the purposes of this study the former is used. ENVI EX also allows you to input existing GIS or field data to supplement the classification.

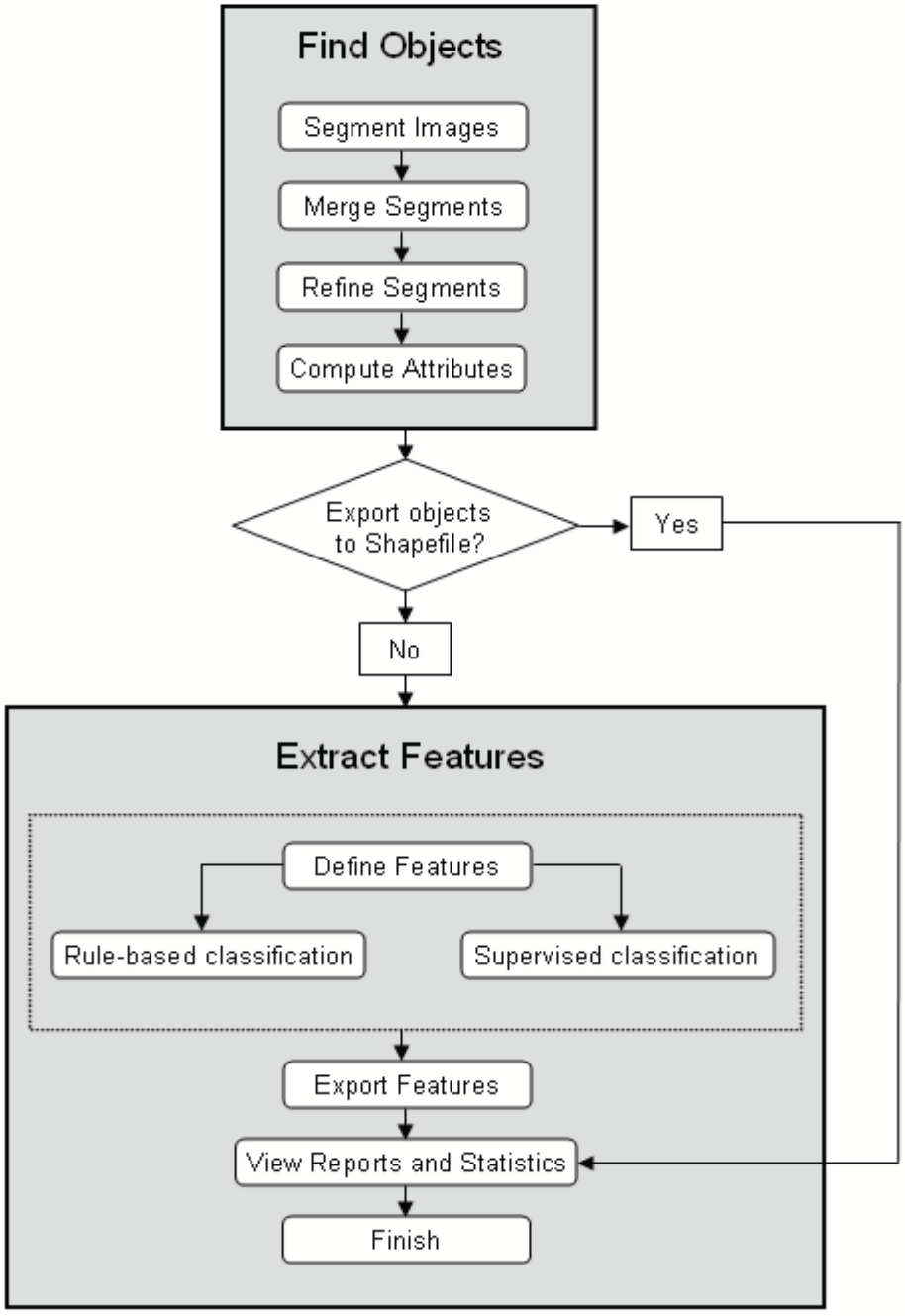

Figure 3. Workflow of the classifications performed in ENVI EX taken from the ENVI EX User Guide

The workflow of the object-oriented classification used here consists of two primary steps: 1) creation of image objects using an image segmentation algorithm that incorporates user-defined scale and merge parameters and 2) supervised classification of the image using the object-based metrics along with any additional ancillary data that the user includes. The creation of image objects in ENVI EX was divided into four steps: Segment, Merge, Refine, and Compute Attributes.

For part two, all of the object attributes computed for each layer will be used for the classification unless specified otherwise by the user. Not all calculated attributes are useful when distinguishing between objects, and the resulting classification may not turn out as accurate if all attributes were used due to the noise introduced by extraneous attributes. ENVI EX provides the option to either manually select the desired attributes to use in the classification, or to "Auto Select Attributes" which is especially useful if you are dealing with a large number of objects. This specification can be done during the supervised classification part by selecting the "Attributes" tab followed by the "Auto Select Attributes" tab.

From here supervised classification was performed using carefully selected training data of each land cover type. The first classification was performed on the imagery alone. The scale was set to 30 with a merge level of 77.7. In ENVI EX, the scale parameter determines the size of the segments that are created on your image to delineate similar groups of pixels that represent the different objects on the landscape. The merge parameter is then used to group segments with adjacent segments that share the same spectral, spatial, and textural characteristics. This helps to mitigate any over-

segmentation. The specific scale and merge values used here were determined through a trial and error process in order to determine the best way to achieve individual tree crown delineation for this particular study site. These parameters were used on all three of the classifications performed here for comparison purposes. In other words, only the image bands were used as input layers in the segmentation and merge process. The lidar layers for the subsequent classifications, including intensity data and height data, were added after the image was segmented into objects.

A k-Nearest Neighbor (k-NN) algorithm was used to assign training segments to feature classes. The k-NN classification method considers the Euclidean distance in n-dimensional space of the object to the elements in the training data, where n is defined by the number of object attributes used during classification. This method is usually more robust than a traditional nearest-neighbor classifier, since the k-nearest distances are used as a majority vote to establish which class the object belongs to. The k-NN method is considerably less sensitive to outliers and noise in the dataset and typically produces a more accurate classification result compared with traditional nearest-neighbor methods (Hsu et. al., 2007).

3.6 Validation Procedures

Remote sensing image classification requires an assement of classification accuracy. Reference data included field visits and high resolution Google Earth imagery. The verification of vegetation types was completed *in situ* while the verification of

developed features was accomplished using Google Earth imagery. To assess the accuracy of the final classifications, sample points were selected using a stratified random sampling design, stratified by land cover class. The number of sample points was calculated using the following equation based on multinomial probability distribution (Jensen, 2005).

$$N = \frac{B\Pi_i(1-\Pi_i)}{b^2_i} \quad (1)$$

where N = number of samples, Π_i is the proportion of a population (number of objects) in the i_{th} class out of k classes with the proportion closest to 50% (in this case urban), b_i is the desired precision (10%), B is the upper (a/k) x 100^{th} percentile of the Chi-square (x^2) distribution with one degree of freedom, and k is the number of classes. To achieve a 90% desired level of confidence and 10 % precision (b_i) of 10%, 150 samples between six classes (25 per class) were required.

Currently, the standard for reporting classification accuracy assessment results focuses on the confusion (or error) matrix, which summarizes the comparison of map class counts with reference class counts. A confusion matrix was created for each of the classification maps. These three matrices were used to to provide a basic description of the classification map accuracies including calculations of producer's accuracy (omission error), user's accuracy (commission error), and overall accuracy (Table 4). The producer's accuracy refers to the percentage of segments of a certain land cover class that are correctly classified as that land cover class, while the user's accuracy refers to the probability that a segment classified on the map actually represents that category on the

ground. The user and producer accuracies for any given class typically are not the same (Jensen, 2005).

A comparison of accuracies between the three maps based on the Kappa coefficient of agreement ($\hat{K}$) for each classification was also performed. This analysis is based on the comparison of the predicted and actual class labels for each case in a reference set and can be calculated from Equation 2.

$$\hat{K} = \frac{P_o - P_c}{1 - P_c} \quad (2)$$

where p_o is the proportion of cases in agreement (i.e., correctly classified segments) and P_c is the proportion of agreement that is expected by chance. The calculated coefficient provides an estimate of the accuracy of the map which together with that derived from another map is the basis of most map comparisons (Foody, 2004).

This comparison also aims to establish whether or not the difference between the classification results produced can be inferred to indicate a statistically significant difference between the associated population parameters of accuracy. Significant differences in Kappa coefficients of agreement were tested by calculating a z score

$$z = \frac{(\hat{k}_1 - \hat{k}_2)}{\sqrt{(\hat{\sigma}^2_{(\hat{k}_1)} + \hat{\sigma}^2_{(\hat{k}_2)})}} \quad (3)$$

where the numerator represents the difference between Kappa coefficients for two different maps, k_1 and k_2, and the denominator represents the square root of the sum of estimated variances of the two Kappa coefficients. To determine if there is a significant

difference between two Kappa coefficients (two-sided test), the null hypothesis of no significant difference would be rejected at the widely used 5 percent level of significance ($\alpha = 0.05$) if the absolute value of z is greater than ± 1.96 (Congalton et al., 1983; Rosenfield and Fitzpatrick-Lins, 1986; Congalton and Green, 1999).

Table 3. Values calculated from the information provided by the confusion matrix

Overall Accuracy	(# samples correctly classified) / (total # of samples)
Producer's Accuracy	(# of samples correctly classified as class A) / (# ground reference samples in class A)
User's Accuracy	(# of samples correctly classified as class A) / (total # of samples classified as class A)

4.0 RESULTS

The classification map using imagery alone is provided in Figures 4. The classification map using imagery and height data is provided in Figure 5, and the classification map using imagery and intensity data is provided in Figure 6. The accuracy results of all three classifications are summarized in Table 4. These z score calculations are provided in Table 5. Interestingly, adding lidar height information to the image data did not increase but decreased the overall classification accuracy. However, adding lidar intensity information did improve the overall classification. Urban vegetation classification using imagery alone resulted in an 83.89 percent overall accuracy. In comparison, imagery plus lidar height data resulted in an overall accuracy of 82.78 percent, and imagery plus intensity information resulted in an overall accuracy of 88.33 percent.

Adding lidar intensity to the classification did increase the overall accuracy by 4.44 percent, however, decreased the Kappa statistic of the broad-leafed evergreen class by 3.18 percent. Adding height to the classification actually decreased the overall classification accuracy by 1.11 percent but increased the Kappa statistic of the broad-leaf evergreen and mixed forest classes by 12.56 percent and 3.94 percent respectively.

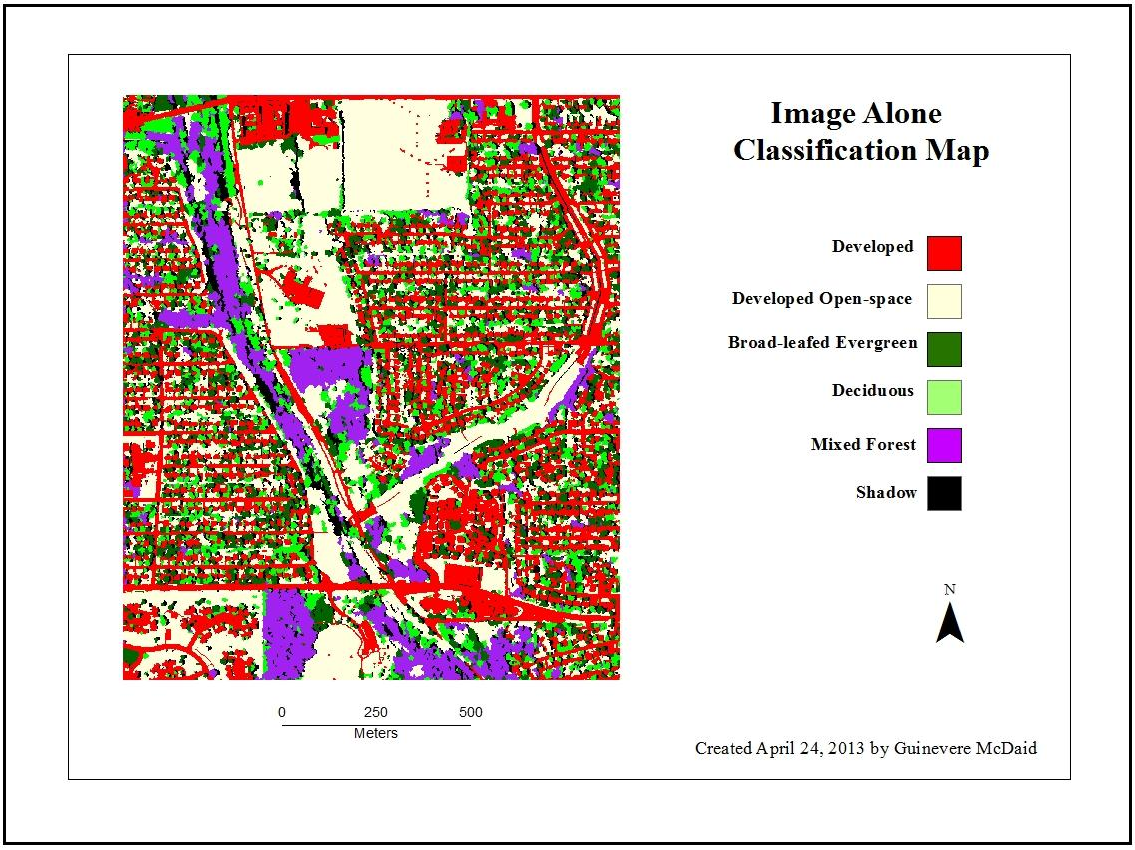

Figure 4. Classification map produced from imagery alone

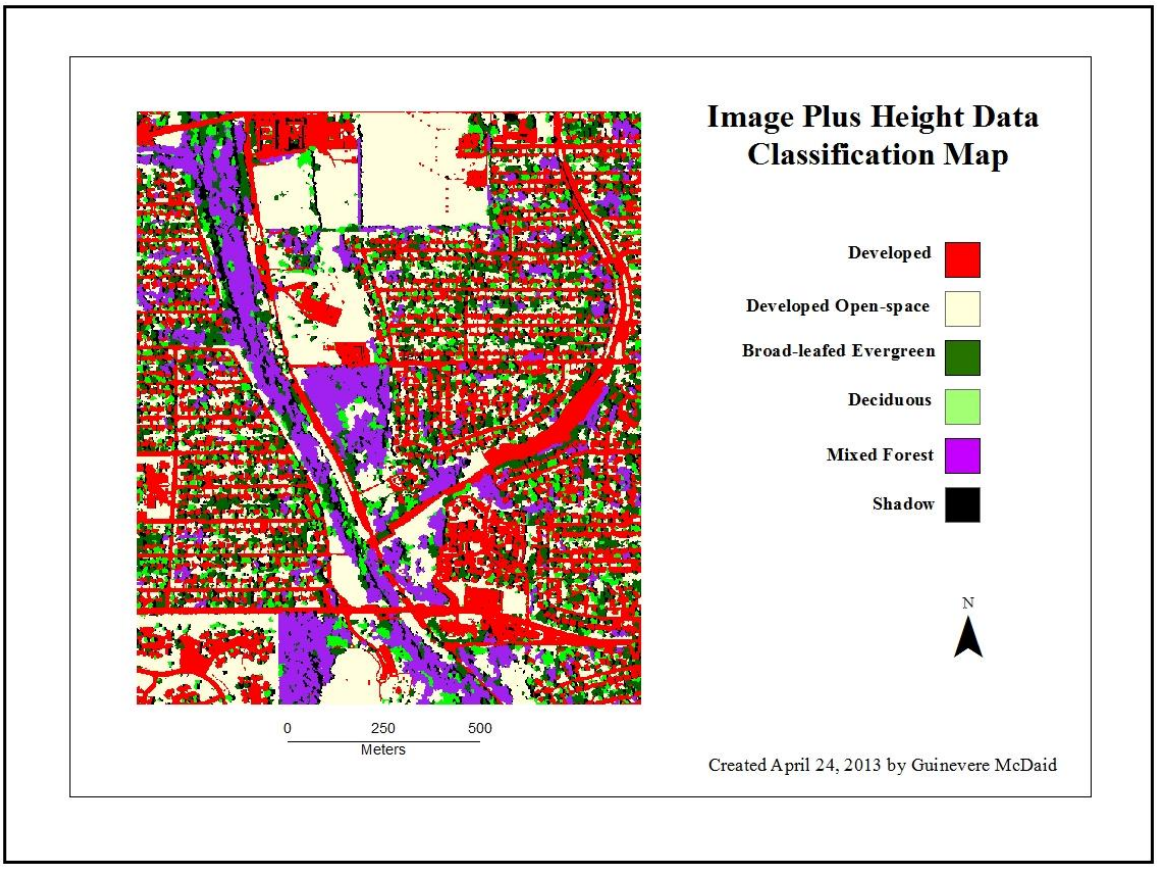

Figure 5. Classification map produced from imagery plus height information

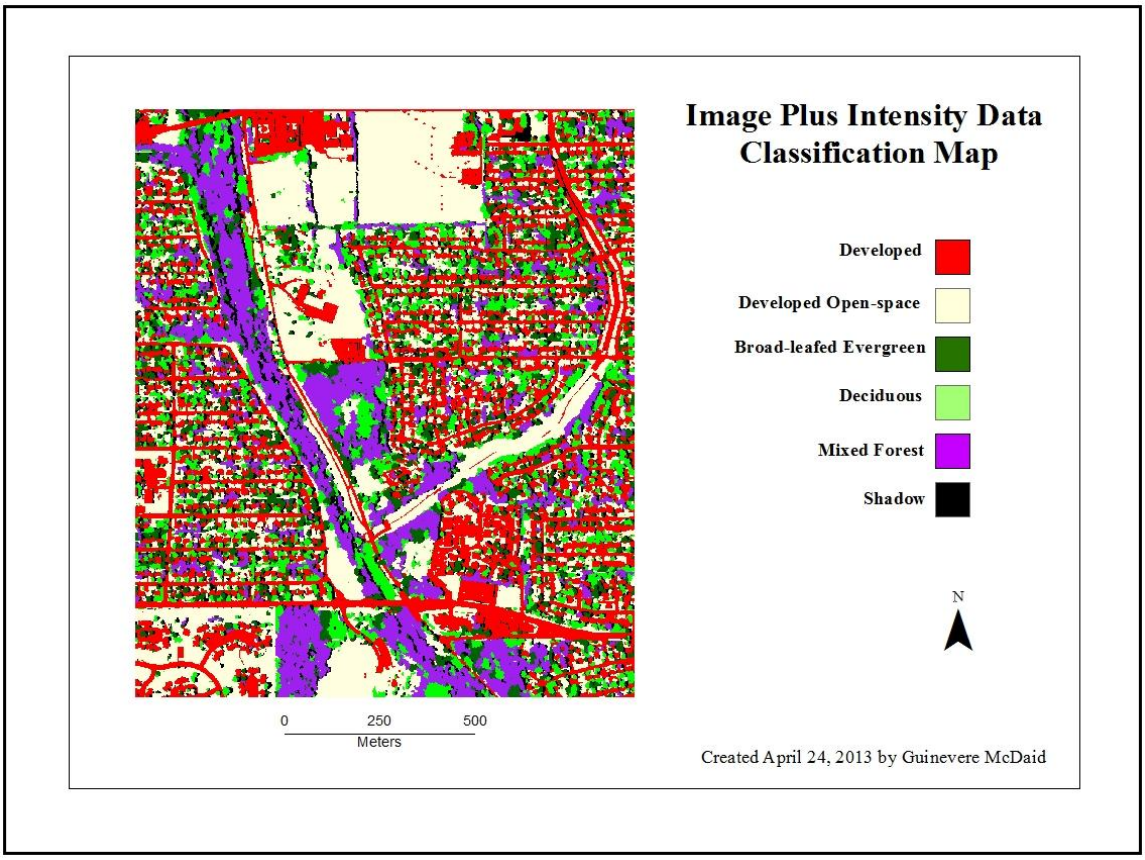

Figure 6. Classification map produced from imagery plus intensity information

Table 4. Accuracy assessment results for all three classifications performed for this study

Classification using imagery alone

Class name	Producer's Accuracy (%)	User's Accuracy (%)	KAPPA Statistic (%)	Overall KAPPA Statistic 80.67%
Developed	96.55	93.33	92.05	
Developed Open-space	75.00	90.00	87.50	
Broad-leafed Evergreen	100	56.67	52.15	Overall Classification Accuracy 83.89%
Cold Deciduous	67.57	83.33	79.02	
Mixed Forest	78.13	83.33	79.73	
Shadow	100	96.67	96.03	

Classification using imagery and lidar derived height information

Class name	Producer's Accuracy (%)	User's Accuracy (%)	KAPPA Statistic (%)	Overall KAPPA Statistic 79.33%
Developed	100	100	100	
Developed Open-space	79.31	76.67	72.19	
Broad-leafed Evergreen	77.78	70.00	64.71	Overall Classification Accuracy 82.78%
Cold Deciduous	63.64	70.00	63.27	
Mixed Forest	78.79	86.67	83.67	
Shadow	100	93.33	92.11	

Classification using imagery and lidar intensity information

Class name	Producer's Accuracy (%)	User's Accuracy (%)	KAPPA Statistic (%)	Overall KAPPA Statistic 86.00%
Developed	100	96.67	96.03	
Developed Open-space	78.95	100	100	Overall Classification Accuracy 88.33%
Broad-leafed Evergreen	85.71	60	54.72	
Cold Deciduous	77.42	80	75.84	
Mixed Forest	96.55	93.33	92.05	
Shadow	93.75	100	100	

Table 5. Kappa Z-tests used to determine if Kappa values from two classifications are significantly different from each other (Congalton and Green, 2008). The null hypothesis is rejected if the Z-statistic is greater than the critical value (1.96 for a 95% confidence level). The p-values for the Z-scores reported here correspond to overall Kappa values for the classifications.

Class	Imagery alone (K1)	Imagery + Intensity (K2)	Z score	P(Z<=z) two-tail
Developed	1	0.9205	1.0864	
Developed Open-space	0.7219	0.8750	0.8250	
Broad-leafed Evergreen	0.6471	0.5215	1.2408	**p value = 0.84**
Deciduous	0.6327	0.7902	0.8007	
Mixed	0.8367	0.7973	1.0494	
Shadow	0.9211	0.9603	0.9592	

Class	Imagery Alone(K1)	Imagery + Height (K2)	Z score	P(Z<=z) two-tail
Developed	1	0.9603	1.0413	
Developed Open-space	0.7219	1	0.7219	
Broad-leafed Evergreen	0.6471	0.5472	1.1826	**p value = 0.46**
Deciduous	0.6327	0.7584	0.8343	
Mixed	0.8367	0.9205	0.9090	
Shadow	0.9211	1	0.9211	

5.0 DISCUSSION

5.1 Segmentation and image classification

The segmentation scale parameter used here was based only on the image bands for all three classifications. Since the scale parameter is the most important factor in determining the object size and shape which in turn decides the maximum heterogeneity allowed between image objects (Chen et al., 2009), it could be argued that segmentation scale parameters based on additional input layers (i.e., height and intensity), could potentially add to the accuracy of these classifications. For example, in Ke et al. (2010), three types of segmentation schemes were evaluated for the purpose of determining which would provide the best object-oriented classification results for various tree types including six different deciduous species and four different coniferous species. They found that classification based solely on objects created from spectral metrics, acquired from high resolution multispectral imagery, produced less accurate results than using object-oriented schemes that were based on both spectral and lidar data combined. They found specifically that the object-oriented scheme that integrated spectral data, lidar height metrics, and lidar topographic metrics resulted in the highest forest classification accuracies. The authors also noted that using lidar-derived topographic and height

information helped reduce the large amounts of within class spectral variation due to relief displacement and the effects of shadows.

5.2 Influence of adding lidar height and intensity information

The overall accuracy and Kappa statistic of the classification using both imagery and lidar height information changed very little from the classification using imagery alone. Using the height layer as input did increase Kappa statistic of the broad-leaf evergreen class and the mixed forest class from 52.15 percent to 64.71 percent and 79.73 percent to 83.67 percent respectively. However the decrease in Kappa statistic of the deciduous class from 79.02 percent to 63.2 percent (a decrease of 15.75 percent) averaged out the increases of those two classes resulting in very little change in overall accuracy between these two classifications. The large decrease in the deciduous class accuracy following the addition of height information could be due to the fact that there are close to a dozen types of deciduous trees within this study area. Of the different species of deciduous trees in this study area, four (*Quercus macrocarpra, Quercus muehlenbergi, Platanus Mexican, and Carya illinoensis*) have a mature canopy height of 45 feet, one (*Quercus buckleyi)* has a mature canopy height of 35 feet, five (*Ulmus crassfolia, Acer grandidentatum, Prosopis glandulosa, Quercus laceyl, and Juglans microcarpa)* have a mature canopy height of 30 feet, and one (*Lagerstroemia indica*) has a mature canopy height of 20 feet. The wide range in maximum canopy heights between the deciduous species could be a source of classification error. Additionally, if the canopy structures of these deciduous trees have a wide range in variation of how their branches are spread and organized, it would make sense that adding a height layer

containing the coefficient of variation to the image classification might confuse the identification of this class.

The specific collection date of the lidar collected over this study area was early October before the leaves on the trees in this particular region fall off. This may have in turn affected the accuracy of the DEMs from which the height calculations used in the classification were based on. In two different studies done by Hodgson et al. (2003) and Hodgdon et al. (2005), it was determined that land cover, in particular higher vegetation types (e.g. forest canopy), strongly influence the accuracy of the lidar elevation. The authors in both studies established a correlation between the density of ground returns for various land cover types and the amount of error in elevation. The further the mean distance between ground returns for each class, the higher the error is in elevation for that class. Tree canopy cover influences the penetration rate of the lidar which consequently confuses the weeding algorithms used to classify the ground points (Hodgdon, 2003) which in turn leads to less accurate DEMs. This could have contributed to the decrease in accuracy of the deciduous classes following the addition of height information due to the broad range in tree heights of the various deciduous species. Since there is only one dominant type of broad-leafed evergreen species in this study area, any error in elevation calculations would arguably be consistent over all broad-leafed evergreens allowing the software to identify a specific height pattern to associate with that class. This could explain why adding height information increased the accuracy of the broad-leafed evergreen class but decreased the deciduous class.

Using leaf-on lidar may have also decreased the value of the additional information that lidar could potentially add to the classification. If lidar acquired during January or February was used, it may have provided the type of information needed to distinguish between deciduous trees from broad-leafed evergreen trees. If further break-down of the deciduous class was explored, then using leaf-off data could be more useful as the vertical distribution, configuration and features of the leaf-off branches within each tree crown has been shown to be species specific (Brandtburg, 2003). Brandtburg used common statistical measurements calculated from lidar height data to evaluate the difference between the vertical distributions of leaf-off branches of three different deciduous tree species. It could also be argued that using imagery acquired during those leaf-off months would have had the same effect as using leaf-off lidar data as far as separating broad-leaf evergreen from deciduous trees. In fact, using imagery collected during the leaf-off time of year might eliminate the need for adding lidar to the study in the first place because there would potentially be a wider range of spectral, spatial and textural variation between deciduous trees and broad-leaf evergreen trees. Lidar and aerial imagery are both expensive forms of data to acquire and often researchers use what data is available for their area of interest which is the case here. Since the NAIP imagery was acquired during the leaf-on period for the trees in this region, using lidar acquired during the leaf-off might have provided better separation between the deciduous class and the broad-leafed evergreen class.

The addition of intensity information to the classification increased the overall accuracy and kappa statistic by 4.40 percent and 5.33 percent respectively. Most of this increase was observed in the mixed forest class which improved from a kappa statistic of

79.73 percent to a 92.05 percent (a 12.32 percent increase). This considerable increase could be due to the increased range of values within this class that the addition of intensity information provided for each sample object that the image data alone did not provide.

Some studies have used lidar information to classify different tree types based on crown shape and or structure (Popescu and Zhao, 2008; Kim et al., 2011; Li et al., 2012), however, in this particular study area, there are many man-made structures and human-behaviors that may influence and/or change the natural shape and structure of tree crowns, like stylistic pruning, power-line interference, adjacent buildings, asphalt, etc. This presents a challenge to establish a consistent pattern that can then be associated with any one tree type for the purpose of classification.

There are several parameters that through further evaluation and or adjustment (ie., segmentation scale, segmentation based on additional input layers, or an increased number of height statistics used) could potentially improve the results here. This study is limited to how the coefficient of variation differs between broad-leaf evergreen class and the deciduous class. This statistic alone may not be sufficient to do distinguish between the two classes, especially when dealing with such a large number of structurally different tree species within the deciduous class and the potential outside factors influencing shape, structure and growth patterns of urban trees.

Of the studies described above that have successfully used height information to improve classifications of various tree types, none of them have dealt with the classification of deciduous trees and broad-leaf evergreen trees where there are close to a

dozen species of one type of tree (ie deciduous) and only one predominant species of the other type of tree (ie, broad-leaf evergreen). Further improvement to this classification might be possible if the deciduous class was broken down into individual species. Otherwise, it might be that the range in structural position of the leaves and branches within the deciduous class is just too wide for a unique pattern to be determined and then used in assigning trees to the deciduous class. The use of additional statistics could also be explored to evaluate the effects on these classification results. Using only the coefficient of variation may not be sufficient to do distinguish between the two classes, especially when dealing with such a heterogeneous urban tree population.

Another possible source of error could be attributed to the presence of noise in the lidar data set as that is known to affect the accuracy of lidar measurements (Fang and Huang, 2004). Further work could be done to improve the results of these classifications by assessing the effectiveness of using different filter algorithms to further clean the lidar data used here. Filtering out extremely high lidar points that were collected over power lines, in-flight birds, and radio towers may provide for more accuracy in the creation of the vegetation class which could in turn potentially improve the image classification when used together. The same could be done for extremely low points that were mistakenly omitted from the ground point classification done by the vendor.

Performing a rule based classification in ENVI EX instead of one that uses the training data to classify could result in an improved classification results. This method would likely require a little more user knowledge of the canopy shape and structure of each tree type in the study area in order to create meaningful rules for the software to base its object classifications on. Experimenting with additional lidar layers that contain

different statistics calculated for each 1 square meter pixel and using as inputs into the image classification may improve the software's ability to separate spectrally similar classes like deciduous and evergreen or even to separate the different deciduous species into their own class. Further experimentation with the segmentation parameter as well as the merge parameters in ENVI EX which would change the shape and size of the objects that the respective lidar points would be associated with could also change how accurately the image could be classified as Ke et al. (2010) demonstrated.

The amount of moisture a plant receives effects the moisture content and chlorophyll content in their leaves which in turn affects how energy is absorbed or reflected within the internal leaf structure. The variation in response between trees of the same class to the energy measured by the sensor can make it difficult for any definitive spectral or spatial characteristics to be associated with any one tree type, thus leading to misclassifications. Also, in a dense urban setting, such as the one used for this research, outside of rainfall, the only water available to urban vegetation is from human provided sources or along riparian areas that maintain a consistent supply of water even in times of drought. Further research into the variability of water availability between trees within urban areas, other than rain fall, would have to be evaluated before claims of uneven water distribution could be claimed as a possible cause of the extreme variation in tree health seen between trees of the same class. For example, in a study done by Nelson et al. (2000) it was determined that variation in tree canopy shape due to insects and drought affected how well lidar-based models could be used to accurately classify individual tree types.

6.0 CONCLUSION

The classification method used here has demonstrated that lidar-derived information did not necessarily improve the urban vegetation classification for downtown San Antonio when added to image data. Adding height information to the image classification actually decreased the overall accuracy of the classification by 1.11. It did prove useful at improving the broadleaf evergreen class yet detrimental to the accuracy of the deciduous class. As mentioned earlier, a possible reason for this could be due to the large number of deciduous species with in the study area. Adding lidar-derived intensity information did lead to an increase in overall classification accuracy as well as a significant increase of to the mixed forest class.

The research presented here represents only a fraction of the extent that could potentially be covered. Due to the two year time limitation of producing a thesis coupled with the steep learning curve of working with lidar and remotely sensed data, this research will stand to serve as a benchmark for future studies.

REFERENCES

Adams, J. B., D. E. Sabol, V. Kapos, R. Almeida Filho, D. A. Roberts, M. O. Smith, and A. R. Gillespie. 1995. Classification of multispectral images based on fractions of endmembers: Application to land-cover change in the Brazilian Amazon. *Remote Sensing of Environment* 52:137-154.

Alonso, M. C., Malpica, J.A. 2008. Classification of Multispectral High-Resolution Satellite Imagery Using LIDAR Elevation Data. ISVC (2) 85-94.

Anderson, J.R., Hardy, E.E., Roach, J. T., Witmer R.E. 1976 A land use and land cover classification system for use with remote sensor data Government Printing Office, Washington, DC (1976) US Geological Survey, Professional Paper 964.

Aniello, C., K. Morgan, A. Busbey, and L. Newland. 1995. Mapping micro-urban heat islands using LANDSAT TM and a GIS. *Computers & Geosciences* 21:965-969.

Antonarakis, A. S., K. S. Richards, and J. Brasington. 2008. Object-based land cover classification using airborne LiDAR. *Remote Sensing of Environment* 112:2988-2998.

Aplin, P., P. M. Atkinson, and P. J. Curran. 1999. Fine Spatial Resolution Simulated Satellite Sensor Imagery for Land Cover Mapping in the United Kingdom. *Remote Sensing of Environment* 68:206-216.

Awrangjeb, M., M. Ravanbakhsh, and C. S. Fraser. 2010. *Automatic Building Detection Using LIDAR Data and Multispectral Imagery.* Paper presented at: Digital Image Computing: Techniques and Applications (DICTA), 2010 International Conference on, pp. 45-51.

Axelsson, P. 1999. Processing of laser scanner data—algorithms and applications. *ISPRS Journal of Photogrammetry and Remote Sensing* 54:138-147.

Barnsley, M. J., and S. L. Barr. 1997. Distinguishing urban land-use categories in fine spatial resolution land-cover data using a graph-based, structural pattern recognition system. *Computers, Environment and Urban Systems* 21:209-225.

Barr, S., and M. Barnsley. 2000. Reducing structural clutter in land cover classifications of high spatial resolution remotely-sensed images for urban land use mapping. *Computers & Geosciences* 26:433-449.

Bork, E. W., and J. G. Su. 2007. Integrating LIDAR data and multispectral imagery for enhanced classification of rangeland vegetation: A meta-analysis. *Remote Sensing of Environment* 111:11-24.

Brandtberg, T., T. A. Warner, R. E. Landenberger, and J. B. McGraw. 2003. Detection and analysis of individual leaf-off tree crowns in small footprint, high sampling density lidar data from the eastern deciduous forest in North America. *Remote Sensing of Environment* 85:290-303.

Brodu, N., and D. Lague. 2012. 3D terrestrial lidar data classification of complex natural scenes using a multi-scale dimensionality criterion: Applications in geomorphology. *ISPRS Journal of Photogrammetry and Remote Sensing* 68:121-134.

Carrão, H., P. Gonçalves, and M. Caetano. 2008. Contribution of multispectral and multitemporal information from MODIS images to land cover classification. *Remote Sensing of Environment* 112:986-997.

Charaniya, R. Manduchi, S.K. Lodha. Supervised parametric classification of aerial LiDAR data CVPRW'04, Proceedings of the IEEE 2004 Conference on Computer Vision and Pattern Recognition Workshop, 27 June – 2 July 2004, Baltimore, Md, Vol. 3 (2004), pp. 1– 8.

Chehata, N., Guo, L., Mallet, C. Airborne LiDAR feature selection for urban classification using random forests International Archives of the Photogrammetry, Remote Sensing and Spatial Information Sciences, 39 (Part 3/W8) (2009), pp. 207–212.

Chen, Y., W. Su, J. Li, and Z. Sun. 2009. Hierarchical object oriented classification using very high resolution imagery and LIDAR data over urban areas. *Advances in Space Research* 43:1101-1110.

Chen, Z., B. Devereux, B. Gao, and G. Amable. 2012. Upward-fusion urban DTM generating method using airborne Lidar data. *ISPRS Journal of Photogrammetry and Remote Sensing* 72:121-130.

Cho, M. A., R. Mathieu, G. P. Asner, L. Naidoo, J. van Aardt, A. Ramoelo, P. Debba, K. Wessels, R. Main, I. P. J. Smit, and B. Erasmus. 2012. Mapping tree species composition in South African savannas using an integrated airborne spectral and LiDAR system. *Remote Sensing of Environment* 125:214-226.

Chormanski, J., T. Okruszko, S. Ignar, O. Batelaan, K. T. Rebel, and M. J. Wassen. 2011. Flood mapping with remote sensing and hydrochemistry: A new method to distinguish the origin of flood water during floods. *Ecological Engineering* 37:1334-1349.

Chust, G., M. Grande, I. Galparsoro, A. Uriarte, and Á. Borja. 2010. Capabilities of the bathymetric Hawk Eye LiDAR for coastal habitat mapping: A case study within a Basque estuary. *Estuarine, Coastal and Shelf Science* 89:200-213.

Clark, M. L., D. B. Clark, and D. A. Roberts. 2004. Small-footprint lidar estimation of sub-canopy elevation and tree height in a tropical rain forest landscape. *Remote Sensing of Environment* 91:68-89.

Clark, M. L., D. A. Roberts, J. J. Ewel, and D. B. Clark. 2011. Estimation of tropical rain forest aboveground biomass with small-footprint lidar and hyperspectral sensors. *Remote Sensing of Environment* 115:2931-2942.

Cobby, D. M., D. C. Mason, and I. J. Davenport. 2001. Image processing of airborne scanning laser altimetry data for improved river flood modelling. *ISPRS Journal of Photogrammetry and Remote Sensing* 56:121-138.

Collin, A., B. Long, and P. Archambault. 2012. Merging land-marine realms: Spatial patterns of seamless coastal habitats using a multispectral LiDAR. *Remote Sensing of Environment* 123:390-399.

———2010. Salt-marsh characterization, zonation assessment and mapping through a dual-wavelength LiDAR. *Remote Sensing of Environment* 114:520-530.

Collins, J. B., and C. E. Woodcock. 1994. Change detection using the Gramm-Schmidt transformation applied to mapping forest mortality. *Remote Sensing of Environment* 50:267-279.

Congalton, R.G., and K. Green, 1999. *Assessing the Accuracy of Remotely Sensed Data: Principles and Practices,* Lewis, Boca Raton, Florida, 137 p.

———2008. *Assesing the Accuracy of Remotely Sensed Data: Principles and Practices (2nd edition),* Boca Raton, Florida, 105-110 p.

Congalton, R.G., R.G. Oderwald, and R.A. Mead, 1983. Assessing Landsat classification accuracy using discrete multivariate analysis statistical techniques, *Photogrammetric Engineering & Remote Sensing* 49:1671–1678.

Culbert, P. D., V. C. Radeloff, V. St-Louis, C. H. Flather, C. D. Rittenhouse, T. P. Albright, and A. M. Pidgeon. 2012. Modeling broad-scale patterns of avian species richness across the Midwestern United States with measures of satellite image texture. *Remote Sensing of Environment* 118:140-150.

Curran, P. J., P. M. Atkinson, G. M. Foody, and E. J. Milton. Linking remote sensing, land cover and disease. In *Advances in Parasitology,* ed. Anonymous 37-80. Academic Press.

Dalponte, M., L. Bruzzone, and D. Gianelle. 2012. Tree species classification in the Southern Alps based on the fusion of very high geometrical resolution multispectral/hyperspectral images and LiDAR data. *Remote Sensing of Environment* 123:258-270.

Danson, F. M., and P. J. Curran. 1993. Factors affecting the remotely sensed response of coniferous forest plantations. *Remote Sensing of Environment* 43:55-65.

Donoghue, D. N. M., P. J. Watt, N. J. Cox, and J. Wilson. 2007. Remote sensing of species mixtures in conifer plantations using LiDAR height and intensity data. *Remote Sensing of Environment* 110:509-522.

Drake, J. B., R. O. Dubayah, D. B. Clark, R. G. Knox, J. B. Blair, M. A. Hofton, R. L. Chazdon, J. F. Weishampel, and S. Prince. 2002. Estimation of tropical forest structural characteristics using large-footprint lidar. *Remote Sensing of Environment* 79:305-319.

DU, P., X. LI, W. CAO, Y. LUO, and H. ZHANG. 2010. Monitoring urban land cover and vegetation change by multi-temporal remote sensing information. *Mining Science and Technology (China)* 20:922-932.

Dutartre, P., J. M. Coudert, and G. Delpont. 1993. Evolution in the use of satellite data for the location and development of groundwater. *Advances in Space Research* 13:187-195.

Eyton, J. R. 1993. Urban land use classification and modelling using cover-type frequencies. *Applied Geography* 13:111-121.

Foody, G.M., 2004. Thematic Map Comparison: Evaluating the statistical significance of differences in classification accuracy. *Photogrametric Engineering and Remote Sensing* 70:627-633.

Forzieri, G., M. Degetto, M. Righetti, F. Castelli, and F. Preti. 2011. Satellite multispectral data for improved floodplain roughness modelling. *Journal of Hydrology* 407:41-57.

Franco-Lopez, H., A. R. Ek, and M. E. Bauer. 2001. Estimation and mapping of forest stand density, volume, and cover type using the k-nearest neighbors method. *Remote Sensing of Environment* 77:251-274.

Froger, J. -., J. -. Lénat, J. Chorowicz, J. -. Le Pennec, J. -. Bourdier, O. Köse, O. Zimitoglu, N. M. Gündogdu, and A. Gourgaud. 1998. Hidden calderas evidenced by multisource geophysical data; example of Cappadocian Calderas, Central Anatolia. *Journal of Volcanology and Geothermal Research* 85:99-128.

Gan, T. Y., F. Zunic, C. -. Kuo, and T. Strobl. 2012. Flood mapping of Danube River at Romania using single and multi-date ERS2-SAR images. *International Journal of Applied Earth Observation and Geoinformation* 18:69-81.

Garcia-Gutierrez, J., L. Gonçalves-Seco, and J. C. Riquelme-Santos. 2011. Automatic environmental quality assessment for mixed-land zones using lidar and intelligent techniques. *Expert Systems with Applications* 38:6805-6813.

Garvin, J., J. Bufton, J. Blair, D. Harding, S. Luthcke, J. Frawley, and D. Rowlands. 1998. Observations of the Earth's topography from the Shuttle Laser Altimeter (SLA): Laser-pulse Echo-recovery measurements of terrestrial surfaces. *Physics and Chemistry of the Earth* 23:1053-1068.

Girel, J., and O. Manneville. 1998. Present species richness of plant communities in alpine stream corridors in relation to historical river management. *Biological Conservation* 85:21-33.

Gross, H., Jutzi, B., Thoennessen, U., Segmentation of tree regions using data of a full-waveform laser. International Archives of the Photogrammetry, Remote Sensing and Spatial Information Sciences, 36 (Part (3/W49A)) (2007), pp. 57–62.

Guo, L., N. Chehata, C. Mallet, and S. Boukir. 2011. Relevance of airborne lidar and multispectral image data for urban scene classification using Random Forests. *ISPRS Journal of Photogrammetry and Remote Sensing* 66:56-66.

Guo, Z., S. D. Wang, M. M. Cheng, and Y. Shu. 2012. Assess the effect of different degrees of urbanization on land surface temperature using remote sensing images. *Procedia Environmental Sciences* 13:935-942.

Gupta, R. K., T. S. Prasad, P. V. Krishna Rao, and P. M. Bala Manikavelu. 2000. Problems in upscaling of high resolution remote sensing data to coarse spatial resolution over land surface. *Advances in Space Research* 26:1111-1121.

Haack, B., and R. English. 1996. National land cover mapping by remote sensing. *World Development* 24:845-855.

Haala, N. 1994. Detection of buildings by fusion of range and image data. *Proceedings of SPIE*341.

Hamada, Y., D. A. Stow, and D. A. Roberts. 2011. Estimating life-form cover fractions in California sage scrub communities using multispectral remote sensing. *Remote Sensing of Environment* 115:3056-3068.

Hardeberg, J. Y. 2006. Recent advances in acquisition and reproduction of multispectral images. *14th European Signal Processing Conference* (EUSIPCO 2006), Florence, Italy, September 4-8, 2006, copyright by EURASIP.

Hartfield, K. A., K. I. Landau, and van Leeuwen, Willem J. D. 2011. Fusion of High Resolution Aerial Multispectral and LiDAR Data: Land Cover in the Context of Urban Mosquito Habitat. *Remote Sensing* 3:2364-2383.

Hay, G. J., G. Castilla, M. A. Wulder, and J. R. Ruiz. 2005. An automated object-based approach for the multiscale image segmentation of forest scenes. *International Journal of Applied Earth Observation and Geoinformation* 7:339-359.

Heinzel, J., and B. Koch. 2011. Exploring full-waveform LiDAR parameters for tree species classification. *International Journal of Applied Earth Observation and Geoinformation* 13:152-160.

Henebry, G. M. 1993. Detecting change in grasslands using measures of spatial dependence with landsat TM data. *Remote Sensing of Environment* 46:223-234.

Hodgson, M. E., J. R. Jensen, J. A. Tullis, K. D. Riordan, and C. M. Archer. 2003. Peer-Reviewed Articles - Synergistic Use of Lidar and Color Aerial Photography for Mapping Urban Parcel Imperviousness - A comparative analysis of pixel-level (maximum-likelihood, ISODATA, and See5) and segment-level (See5) classifiers is presented for mapping urban parcel imperviousness from color aerial photography fused with lidar-derived cover height. *Photogrammetric engineering and remote sensing.* 69:973.

Hodgson, M. E., J. R. Jensen, L. Schmidt, S. Schill, and B. Davis. 2003. An evaluation of LIDAR- and IFSAR-derived digital elevation models in leaf-on conditions with USGS level 1 and level 2 DEMs. *Remote Sensing of Environment* 84, no. 2: 295-308.

Hodgson, M.E., J.R. Jensen, G. Raber, J. Tullis, B. Davis, K. Schuckman, G. Thompson. 2005. An Evaluation of LIDAR-Derived Elevation and Terrain Slope in Leaf-off Conditions, Photogrammetric Engineering and Remote Sensing, 71(1): 817-823.

Höfle, B. & Hollaus, M. 2010: Urban vegetation detection using high density full-waveform airborne LiDAR data - Combination of object-based image and point cloud analysis. In: *International Archives of Photogrammetry, Remote Sensing and Spatial Information Sciences*. Vol. XXXVIII(Part 7B), pp. 281-286.

Höfle, B., M. Hollaus, and J. Hagenauer. 2012. Urban vegetation detection using radiometrically calibrated small-footprint full-waveform airborne LiDAR data. *ISPRS Journal of Photogrammetry and Remote Sensing* 67:134-147.

Hofton, M. A., L. E. Rocchio, J. B. Blair, and R. Dubayah. 2002. Validation of Vegetation Canopy Lidar sub-canopy topography measurements for a dense tropical forest. *Journal of Geodynamics* 34:491-502.

Holmgren, J., and Å. Persson. 2004. Identifying species of individual trees using airborne laser scanner. *Remote Sensing of Environment* 90:415-423.

Hsu, C.-W., C.-C. Chang, and C.-J. Lin. 2007. A practical guide to support vector classification. National Taiwan University. http://ntu.csie.org/~cjlin/papers/guide/guide.pdf.

Huang, X., L. P. Zhang, and W. Gong. 2011. Information fusion of aerial images and LIDAR data in urban areas: vector-stacking, re-classification and post-processing approaches. *International Journal of Remote Sensing* 32:69-84.

Imhoff, M. L., T. D. Sisk, A. Milne, G. Morgan, and T. Orr. 1997. Remotely sensed indicators of habitat heterogeneity: Use of synthetic aperture radar in mapping vegetation structure and bird habitat. *Remote Sensing of Environment* 60:217-227.

Jacquin, A., L. Misakova, and M. Gay. 2008. A hybrid object-based classification approach for mapping urban sprawl in periurban environment. *Landscape and Urban Planning* 84:152-165.

Jensen, J. L. R., K. S. Humes, A. T. Hudak, L. A. Vierling, and E. Delmelle. 2011. Evaluation of the MODIS LAI product using independent lidar-derived LAI: A case study in mixed conifer forest. *Remote Sensing of Environment* 115:3625-3639.

Jensen, J. L. R., K. S. Humes, L. A. Vierling, and A. T. Hudak. 2008. Discrete return lidar-based prediction of leaf area index in two conifer forests. *Remote Sensing of Environment* 112:3947-3957.

Jensen, J.R. 2005, (third edition). *Introductory Digital Image Processing,* Prentice-Hall, Englewood Cliffs, New Jersey, p. 505-506.

Jones, T. G., N. C. Coops, and T. Sharma. 2010. Assessing the utility of airborne hyperspectral and LiDAR data for species distribution mapping in the coastal Pacific Northwest, Canada. *Remote Sensing of Environment* 114:2841-2852.

Kabolizade, M., H. Ebadi, and S. Ahmadi. 2010. An improved snake model for automatic extraction of buildings from urban aerial images and LiDAR data. *Computers, Environment and Urban Systems* 34:435-441.

Kadmon, R., and R. Harari-Kremer. 1999. Studying Long-Term Vegetation Dynamics Using Digital Processing of Historical Aerial Photographs. *Remote Sensing of Environment* 68:164-176.

Kargel, J. S., M. J. Abrams, M. P. Bishop, A. Bush, G. Hamilton, H. Jiskoot, A. Kääb, H. H. Kieffer, E. M. Lee, F. Paul, F. Rau, B. Raup, J. F. Shroder, D. Soltesz, D. Stainforth, L. Stearns, and R. Wessels. 2005. Multispectral imaging contributions to global land ice measurements from space. *Remote Sensing of Environment* 99:187-219.

Katra, I., and N. Lancaster. 2008. Surface-sediment dynamics in a dust source from spaceborne multispectral thermal infrared data. *Remote Sensing of Environment* 112:3212-3221.

Ke, Y., L. J. Quackenbush, and J. Im. 2010. Synergistic use of QuickBird multispectral imagery and LIDAR data for object-based forest species classification. *Remote Sensing of Environment* 114:1141-1154.

Khoshelham, K., C. Nardinocchi, E. Frontoni, A. Mancini, and P. Zingaretti. 2010. Performance evaluation of automated approaches to building detection in multi-source aerial data. *ISPRS Journal of Photogrammetry and Remote Sensing* 65:123-133.

Kim, S., T. Hinckley, and D. Briggs. 2011. Classifying individual tree genera using stepwise cluster analysis based on height and intensity metrics derived from airborne laser scanner data. *Remote Sensing of Environment* 115:3329-3342.

Kim, S., R. J. McGaughey, H. Andersen, and G. Schreuder. 2009. Tree species differentiation using intensity data derived from leaf-on and leaf-off airborne laser scanner data. *Remote Sensing of Environment* 113:1575-1586.

Kruse, F. A., A. B. Lefkoff, and J. B. Dietz. 1993. Expert system-based mineral mapping in northern death valley, California/Nevada, using the Airborne Visible/Infrared Imaging Spectrometer (AVIRIS). *Remote Sensing of Environment* 44:309-336.

Lambin, E. F., and A. H. Strahlers. 1994. Change-vector analysis in multitemporal space: A tool to detect and categorize land-cover change processes using high temporal-resolution satellite data. *Remote Sensing of Environment* 48:231-244.

Lefsky, M.A., W.B. Cohen, G.G. Parker and D.J. Harding. 2002. Lidar remote sensing for ecosystem studies. *Bioscience* 52: 19-30.

Lefsky, M. A., W. B. Cohen, S. A. Acker, G. G. Parker, T. A. Spies, and D. Harding. 1999. Lidar Remote Sensing of the Canopy Structure and Biophysical Properties of Douglas-Fir Western Hemlock Forests. *Remote Sensing of Environment* 70:339-361.

Lévesque, J., and D. J. King. 2003. Spatial analysis of radiometric fractions from high-resolution multispectral imagery for modeling individual tree crown and forest canopy structure and health. *Remote Sensing of Environment* 84:589-602.

Lillesand, T.M. and R.W. Kiefer 1987. *Remote Sensing and Image Interpretation*. Wiley, New York, 1987.

Liu, J., J. Shen, R. Zhao, and S. Xu. 2008. Extraction of individual tree crowns from airborne LiDAR data in human settlements. *Mathematical and Computer Modeling*.

Lu, D., and Q. Weng. 2006. Use of impervious surface in urban land-use classification. *Remote Sensing of Environment* 102:146-160.

Madugundu, R., V. Nizalapur, and C. S. Jha. 2008. Estimation of LAI and above-ground biomass in deciduous forests: Western Ghats of Karnataka, India. *International Journal of Applied Earth Observation and Geoinformation* 10:211-219.

Mallet, C., Bretar, F. and Soergel, U., 2008. Analysis of full-waveform lidar data for classification of urban areas. *Photogrammetrie Fernerkundung GeoInformation* (PFG) 5, pp. 337–349.

Mallet, C., F. Bretar, M. Roux, U. Soergel, and C. Heipke. 2011. Relevance assessment of full-waveform lidar data for urban area classification. *ISPRS Journal of Photogrammetry and Remote Sensing* 66:S71-S84.

Mantovani, F., R. Soeters, and C. J. Van Westen. 1996. Remote sensing techniques for landslide studies and hazard zonation in Europe. *Geomorphology* 15:213-225.

Martin, M. E., S. D. Newman, J. D. Aber, and R. G. Congalton. 1998. Determining Forest Species Composition Using High Spectral Resolution Remote Sensing Data. *Remote Sensing of Environment* 65:249-254.

McGovern, E. A., N. M. Holden, S. M. Ward, and J. F. Collins. 2000. Remotely sensed satellite imagery as an information source for industrial peatlands management. *Resources, Conservation and Recycling* 28:67-83.

McIntosh, K., and A. Krupnik. 2002. Integration of laser-derived DSMs and matched image edges for generating an accurate surface model. *ISPRS Journal of Photogrammetry and Remote Sensing* 56:167-176.

Means, J. E., S. A. Acker, D. J. Harding, J. B. Blair, M. A. Lefsky, W. B. Cohen, M. E. Harmon, and W. A. McKee. 1999. Use of Large-Footprint Scanning Airborne Lidar To Estimate Forest Stand Characteristics in the Western Cascades of Oregon. *Remote Sensing of Environment* 67:298-308.

Mena, J. B., and J. A. Malpica. 2005. An automatic method for road extraction in rural and semi-urban areas starting from high resolution satellite imagery. *Pattern Recognition Letters* 26:1201-1220.

Meng X., Currit N., Zhao K. 2010. Ground Filtering Algorithms for Airborne LiDAR Data: A Review of Critical Issues. *Remote Sensing*. 2(3):833-860.Miller, R. L., and J. F. Cruise. 1995. Effects of suspended sediments on coral growth: Evidence from remote sensing and hydrologic modeling. *Remote Sensing of Environment* 53:177-187.

Muller, E. 1997. Mapping riparian vegetation along rivers: old concepts and new methods. *Aquatic Botany* 58:411-437.

Myint, S. W., P. Gober, A. Brazel, S. Grossman-Clarke, and Q. Weng. 2011. Per-pixel vs. object-based classification of urban land cover extraction using high spatial resolution imagery. *Remote Sensing of Environment* 115:1145-1161.

Niemann, O. 1993. Automated forest cover mapping using thematic mapper images and ancillary data. *Applied Geography* 13:86-95.

Onishi, A., X. Cao, T. Ito, F. Shi, and H. Imura. 2010. Evaluating the potential for urban heat-island mitigation by greening parking lots. *Urban Forestry & Urban Greening* 9:323-332.

Packalén, P., and M. Maltamo. 2007. The k-MSN method for the prediction of species-specific stand attributes using airborne laser scanning and aerial photographs. *Remote Sensing of Environment* 109:328-341.

Phinn, S., M. Stanford, P. Scarth, A. T. Murray, and P. T. Shyy. 2002. Monitoring the composition of urban environments based on the vegetation-impervious surface-soil (VIS) model by subpixel analysis techniques. *International Journal of Remote Sensing* 23:4131-4153.

Pickup, G., V. H. Chewings, and D. J. Nelson. 1993. Estimating changes in vegetation cover over time in arid rangelands using landsat MSS data. *Remote Sensing of Environment* 43:243-263.

Pignatti, S., R. M. Cavalli, V. Cuomo, L. Fusilli, S. Pascucci, M. Poscolieri, and F. Santini. 2009. Evaluating Hyperion capability for land cover mapping in a fragmented ecosystem: Pollino National Park, Italy. *Remote Sensing of Environment* 113:622-634.

Pons, X., and L. Solé-Sugrañes. 1994. A simple radiometric correction model to improve automatic mapping of vegetation from multispectral satellite data. *Remote Sensing of Environment* 48:191-204.

Popescu, S. C., and K. Zhao. 2008. A voxel-based lidar method for estimating crown base height for deciduous and pine trees. *Remote Sensing of Environment* 112:767-781.

Puttonen, E., J. Suomalainen, T. Hakala, E. Räikkönen, H. Kaartinen, S. Kaasalainen, and P. Litkey. 2010. Tree species classification from fused active hyperspectral reflectance and LIDAR measurements. *Forest Ecology and Management* 260:1843-1852.

Rees, W. G., M. Williams, and P. Vitebsky. 2003. Mapping land cover change in a reindeer herding area of the Russian Arctic using Landsat TM and ETM+ imagery and indigenous knowledge. *Remote Sensing of Environment* 85:441-452.

Ridd, M. K., and J. Liu. 1998. A Comparison of Four Algorithms for Change Detection in an Urban Environment. *Remote Sensing of Environment* 63:95-100.

Rosenfield, G.H., and K. Fitzpatrick-Lins, 1986. A measure of agreement as a measure of thematic classification accuracy, *Photogrammetric Engineering & Remote Sensing* 52:223–227.

Rottensteiner, F., J. Trinder, S. Clode, and K. Kubik. 2003. *Building Detection Using LIDAR Data and Multispectral Images.* Paper presented at: Proceedings of the Seventh Biennial Australian Pattern Recognition Society Conference, 10-12 December, 2003, Sidney: CSIRO, pp. 673-682.

Rottensteiner, F., J. Trinder, S. Clode, and K. Kubik. 2007. Building detection by fusion of airborne laser scanner data and multi-spectral images: Performance evaluation and sensitivity analysis. *ISPRS Journal of Photogrammetry and Remote Sensing* 62:135-149.

———2005. Using the Dempster–Shafer method for the fusion of LIDAR data and multi-spectral images for building detection. *Information Fusion* 6:283-300.

Rutzinger, M., B. Höfle, M. Hollaus, and N. Pfeifer. 2008. Object-based point cloud analysis of full-waveform airborne laser scanning data for urban vegetation classification. *Sensors* 8:4505-4528.

Schneider, A. 2012. Monitoring land cover change in urban and peri-urban areas using dense time stacks of Landsat satellite data and a data mining approach. *Remote Sensing of Environment* 124:689-704.

Singh, R. P., K. K. Pahuja, and R. S. Chandel. 1993. Geomorphological features using MSS and TM data. *Advances in Space Research* 13:129-134.

Song, J. H., Han, S. H., Yu, K. Y., Kim, Y. I. 2002. Assessing the possibility of land-cover classification using lidar intensity data. Photogrammetric Computer Vision Symposium 2002, ISPRS Commission III, 9 – 13 September 2002, Graz, Austria, Vol. B, pp. 259–263.

Stefanov, W. L., M. S. Ramsey, and P. R. Christensen. 2001. Monitoring urban land cover change: An expert system approach to land cover classification of semiarid to arid urban centers. *Remote Sensing of Environment* 77:173-185.

Stow, D., Y. Hamada, L. Coulter, and Z. Anguelova. 2008. Monitoring shrubland habitat changes through object-based change identification with airborne multispectral imagery. *Remote Sensing of Environment* 112:1051-1061.

Straatsma, M. W., and M. J. Baptist. 2008. Floodplain roughness parameterization using airborne laser scanning and spectral remote sensing. *Remote Sensing of Environment* 112:1062-1080.

Streutker, D. R., and N. F. Glenn. 2006. LiDAR measurement of sagebrush steppe vegetation heights. *Remote Sensing of Environment* 102:135-145.

Stuckens, J., P. R. Coppin, and M. E. Bauer. 2000. Integrating Contextual Information with per-Pixel Classification for Improved Land Cover Classification. *Remote Sensing of Environment* 71:282-296.

Suárez, J. C., C. Ontiveros, S. Smith, and S. Snape. 2005. Use of airborne LiDAR and aerial photography in the estimation of individual tree heights in forestry. *Computers & Geosciences* 31:253-262.

Sugumaran, R., and M. Voss. 2007. *Object-Oriented Classification of LIDAR-Fused Hyperspectral Imagery for Tree Species Identification in an Urban Environment.* Paper presented at: Urban Remote Sensing Joint Event, 2007, pp. 1-6.

Telfer, B. A., H. H. Szu, and R. K. Kiang. 1993. Classifying multispectral data by neural networks. *Telematics and Informatics* 10:209-222.

Thoreau, R. T., N. C. Coops, N. R. Goodwin, and J. A. Voogt. 2009. Extracting urban vegetation characteristics using spectral mixture analysis and decision tree classifications. *Remote Sensing of Environment* 113:398-407.

Tooke, T. R., N. C. Coops, and J. A. Voogt. 2009. *Assessment of urban tree shade using fused LIDAR and high spatial resolution imagery.* Paper presented at: Urban Remote Sensing Event, 2009 Joint, pp. 1-6.

Townsend, P. A., and S. J. Walsh. 1998. Modeling floodplain inundation using an integrated GIS with radar and optical remote sensing. *Geomorphology* 21:295-312.

Tulldahl, H. M., and S. A. Wikström. 2012. Classification of aquatic macrovegetation and substrates with airborne lidar. *Remote Sensing of Environment* 121:347-357.

van der Linden, S., and P. Hostert. 2009. The influence of urban structures on impervious surface maps from airborne hyperspectral data. *Remote Sensing of Environment* 113:2298-2305.

Vosselman, G., and H. Maas. 2001. Adjustment and filtering of raw laser altimetry data. 62-72.

Vu, T. T., F. Yamazaki, and M. Matsuoka. 2009. Multi-scale solution for building extraction from LiDAR and image data. *International Journal of Applied Earth Observation and Geoinformation* 11:281-289.

Wagner, W., M. Hollaus, C. Briese, and V. Ducic. 2008. 3D vegetation mapping using small-footprint full-waveform airborne laser scanners. *International Journal of Remote Sensing* 29:1433-1452.

Walsh, S. J., D. R. Butler, and G. P. Malanson. 1998. An overview of scale, pattern, process relationships in geomorphology: a remote sensing and GIS perspective. *Geomorphology* 21:183-205.

Wedding, L. M., A. M. Friedlander, M. McGranaghan, R. S. Yost, and M. E. Monaco. 2008. Using bathymetric lidar to define nearshore benthic habitat complexity: Implications for management of reef fish assemblages in Hawaii. *Remote Sensing of Environment* 112:4159-4165.

Weng, Q., D. Lu, and J. Schubring. 2004. Estimation of land surface temperature–vegetation abundance relationship for urban heat island studies. *Remote Sensing of Environment* 89:467-483.

Wentz, E. A., W. L. Stefanov, C. Gries, and D. Hope. 2006. Land use and land cover mapping from diverse data sources for an arid urban environments. *Computers, Environment and Urban Systems* 30:320-346.

Winker, D. M., and M. A. Vaughan. 1994. Vertical distribution of clouds over Hampton, Virginia observed by lidar under the ECLIPS and FIRE ETO programs. *Atmospheric Research* 34:117-133.

Yan, W. Y., A. Shaker, A. Habib, and A. P. Kersting. 2012. Improving classification accuracy of airborne LiDAR intensity data by geometric calibration and radiometric correction. *ISPRS Journal of Photogrammetry and Remote Sensing* 67:35-44.

Yao, W., P. Krzystek, and M. Heurich. 2012. Tree species classification and estimation of stem volume and DBH based on single tree extraction by exploiting airborne full-waveform LiDAR data. *Remote Sensing of Environment* 123:368-380.

Yu, X., J. Hyyppä, M. Vastaranta, M. Holopainen, and R. Viitala. 2011. Predicting individual tree attributes from airborne laser point clouds based on the random forests technique. *ISPRS Journal of Photogrammetry and Remote Sensing* 66:28-37.

Zanganeh Shahraki, S., D. Sauri, P. Serra, S. Modugno, F. Seifolddini, and A. Pourahmad. 2011. Urban sprawl pattern and land-use change detection in Yazd, Iran. *Habitat International* 35:521-528.

Zhang, Y. 1999. Optimisation of building detection in satellite images by combining multispectral classification and texture filtering. *ISPRS Journal of Photogrammetry and Remote Sensing* 54:50-60.

Zhou, G., C. Song, J. Simmers, and P. Cheng. 2004. Urban 3D GIS From LiDAR and digital aerial images. *Computers & Geosciences* 30:345-353.

Zhou, W., G. Huang, A. Troy, and M. L. Cadenasso. 2009. Object-based land cover classification of shaded areas in high spatial resolution imagery of urban areas: A comparison study. *Remote Sensing of Environment* 113:1769-1777.

VITA

Guinevere McDaid was born in Kongsvinger, Norway, on June 8, 1979, the daughter of Susan Bennett McDaid and Brendan Gabriel McDaid. After completing her work at Social Circle High School, Social Circle Georgia, in 1997, she moved around the southern part of the United States working various jobs including exercising race horses, working as an animal control officer and then as a wildlife removal technician before enrolling at Texas State University-San Marcos in 2007. She majored in Geography for her undergraduate degree where she discovered her passion for remote sensing and decided to continue on for a graduate degree.

Permanent Email Address: guinmcdaid@gmail.com

This thesis was typed by Guinevere McDaid.